Materials Advances

ROYAL SOCIETY OF CHEMISTRY

PAPER

View Article Online
View Journal | View Issue

Cite this: *Mater. Adv.*, 2023, 4, 3603

Design and synthesis of hydrophobic mixed organogels with complementary hydrogen-bond donor–acceptor sites: removal of heavy metal ions Hg^{2+}, Cd^{2+} and Pb^{2+} from aqueous solution†

Reena Kyarikwal, [a] Ritika Munjal, [a] Probal Nag, [b] Sivaranjana Reddy Vennapusa [b] and Suman Mukhopadhyay *[a]

Gels, an intermediate state between a solid and liquid, are attracting attention due to the immense possibilities of their potential applications in various fields. Various non-covalent interactions play essential roles in imparting gel strength and stability. Though incorporating metal ions in gelator systems can generate different kinds of metallogels, capturing heavy metal ions using gel structures has scarcely been investigated by researchers. Previously, one low molecular weight gelator (LMWG) molecule *viz.* N^2,N^4,N^6-tri(1*H*-tetrazol-5-yl)-1,3,5-triazine-2,4,6-triamine (**G8**) was introduced by us for discriminating between various isomers of aminopyridines. However, the gel strength was found to be moderate, and it was unstable in water. Herein, we introduced another molecule *viz.* 3,3′,3″-(benzenetricarbonyl-tris(azanediyl))tris(4-aminobenzoic acid) (**GE**) along with **G8** to impart greater stability and make the mixed-gel water stable. The design of the **GE** ensures the presence of complementary hydrogen bond donor–acceptor sites with respect to **G8**. The resultant organogel **G8GE** has shown the ability to form metallogels with Hg(II), Cd(II), and Pb(II) salts. The hydrophobic nature of the gel **G8GE** is observed with the retention of the disc-shaped gel structure in an aqueous medium for an extended period. Metallogels were fabricated with two different methods *viz.* mixing and adsorption methods. Several experiments indicated that in the adsorption method, slow diffusion of metal ions does not disturb the interactions between **G8** and **GE** substantially, proving it to be a more efficient process for gel formation. DFT-based optimization of the structure supports the complementary hydrogen bond formation hypothesis between **G8** and **GE**. The mixed organogel **G8GE** shows the capacity to efficiently remove chloride, acetate, and sulphate salts of toxic metal ions like Hg(II), Cd(II), and Pb(II) from their aqueous solutions. The xerogel **G8GE** adsorbs 56.27% of mercury chloride, 99.24% of mercury acetate, 99.90% of mercury sulphate, 51.83% of cadmium chloride, 98.68% of cadmium acetate, 84.47% of cadmium sulphate, 59.70% of lead chloride and 99.90% of lead acetate and the adsorption capacities (q_e) are 76.24, 157.79, 147.81, 52.09, 131.25, 284.93, 83 and 221.02 mg g^{-1}, respectively. The adsorbent material, *i.e.*, xerogel **G8GE** can be reused for five cycles with 97–99% recovery of the xerogel for further water remediation by treating the mercury-contained mixed organogel with excess KI.

Received 14th June 2023,
Accepted 13th July 2023

DOI: 10.1039/d3ma00300k

rsc.li/materials-advances

1. Introduction

The serendipitous formation of gels with ample balance between different covalent and non-covalent interactions between low molecular weight gelators (LMWGs) and solvent molecules presents a new opportunity to utilize the intermediate state in favour of various applications in diverse fields. Gel formation is a unique property for some organic molecules or inorganic metal complexes.[1] Although it is difficult to precisely predict the structure of a molecule that can form a gel, it can be hypothesised that molecules with certain functional groups and suitable sites for extensive non-covalent interactions can show an increased propensity for the formation of an organogel or metallogel. Organic molecules with carboxamide and tetrazole moieties have shown greater tendencies to form a gel.[2–5] While gels have been seen to have prospective applications in

[a] *Department of Chemistry, School of Basic Science, Indian Institute of Technology Indore, Khandwa Road, Simrol, Indore, 453552, India. E-mail: suman@iiti.ac.in; Fax: +91 731 2361 482; Tel: +91 731 2438 735*

[b] *School of Chemistry, Indian Institute of Science Education and Research Thiruvananthapuram, Thiruvananthapuram 695551, India*

† Electronic supplementary information (ESI) available: Experimental details, spectroscopic characterization, rheological data, and additional supplementary figures. See DOI: https://doi.org/10.1039/d3ma00300k

tissue engineering,[6,7] sensing,[8,9] drug delivery,[10,11] self-healing materials,[12,13] *etc.*, incorporating metal ions into a gel structure can further enrich the materialistic properties by introducing optical,[14,15] magnetic,[16,17] catalytic,[18–20] and conductive properties.[21,22] Interestingly, though LMWGs have shown extensive metallogel formation properties, there are only limited reports where LMWGs are being used in water remediation through the adsorption of heavy metals. However, there are some reports where alginate or cellulose-based gels[23–25] have been used for water remediation. Recently a metalloprotein-based hybrid hydrogel was reported for Cd(II) removal.[26] Some other reports used a glucolipid biosurfactant or a cryogel for heavy metal removal from wastewater.[27–29] These limited studies of heavy metal removal by gel materials are basically related to polymeric gels or high molecular weight gels. Therefore, in this report, the introduction of a modified hydrophobic LMW organogel with a second component has been used for water remediation with increased adsorption capacity as compared to previous limited reports. One major challenge to utilizing gels for water remediation is to stabilize the gels in the presence of excess water. Furthermore, the interactions of metal ions with a gelator system could be of two different types. One could be through forming covalent bonds and making coordination complexes, and the other could be loosely bound metal ions, mainly through non-covalent interactions. In the first case, recovering the heavy metal ions will be difficult after the initial adsorption. So, for an application like water remediation, non-covalent interactions between gel materials and metal ions can be more helpful.

Out of the many contaminants in water, heavy metal salts in water can have very serious effects on human health. Heavy metals are considered to be those with a density of 5 gm cm^{-3} or more.[30] These are found to be toxic and carcinogenic, even at very low concentrations. This pollution mainly originates from the dumping of animal manure, sewage sludge, fertilizer, petroleum distillates waste, and pesticides. Many studies noted hazards of heavy metal impurities like Hg, Cd, Cu, Pb, Zn, *etc.*, in contaminated water,[31,32] out of which the impurities of mercury, cadmium, and lead are the major health concerns for life. Hg^{2+} can damage the nervous system and kidneys, Cd^{2+} can cause damage to kidneys, bones, liver, and blood with its continuous exposure, and Pb^{2+} causes damage to kidneys and liver, and learning difficulties.[33] As purification methods, adsorption by porous materials, membrane separation, electricity driven removal, and several other chemical processes have been reported.[34] Adsorption is the main method because it has no side product formation and is easy to prepare. Some notable ligand-based composite materials and optical sensors have also been reported to detect and remove Pb(II) and Cd(II) ions from contaminated water.[35–41] With our constant endeavours to investigate metallogel formations and properties,[42–45] we have tested the potential applications of utilizing LMWGs for water remediation through heavy metal adsorption. With a porous network that entraps solvent molecules, gels provide attractive scaffolds that capture various ions and molecules within the cavity, particularly when the entrapped solvent is driven off.[34] This can open the door to utilizing gels in environmental applications, specifically water remediation. Removing heavy metal ions from water is an important aspect that has been extensively studied recently.[25–28] However, while employing gels for such applications, it is required to fabricate a robust material that is not soluble in water, even partially.

Recently, we have reported one LMWG *viz.* N^2,N^4,N^6-tri-(1*H*-tetrazol-5-yl)-1,3,5-triazine-2,4,6-triamine (**G8**), which can be utilized to discriminate between isomers of amino pyridines through fluorometric investigations.[46] Interestingly the gel strength of **G8** is found to be moderate. However, **G8** is found to be non-stable when treated with excess water. This might be due to the presence of non-hydrogen bonded tetrazole rings in the periphery that interact extensively with excess water. It is strategized that the incorporation of a second organic molecule with hydrogen-bond donor–acceptor sites complementary to **G8** may enhance the gel strength and stability in water by reducing the excessive hydrogen bond interactions of **G8**. With this background a new molecule *viz.* 3,3′,3″-(benzene-tricarbonyltris(azanediyl))tris(4-aminobenzoic acid) (**Gel Enhancer** or **GE**) has been designed and synthesized. This work discusses the effect on gel formation and properties with **G8** in the presence of equimolar amounts of **GE**. As the resultant organogel is found to be stable in water, it tends to form metallogels with toxic heavy metal ions like Hg(II), Cd(II), and Pb(II); the gel was explored for capturing these heavy metal ions from their aqueous solutions as an effort towards water remediation. Interestingly, during the adsorption study, the properties of metallogels obtained were found to vary with different methods adopted for gel fabrication. Slow diffusion of metal ions through the gel was found to be more efficient than mixing the gelators and metal ions for the fabrication of metallogels in terms of the strength and stability of the resultant gels. We did not find any previous literature report where the modified hydrophobic organogel was used to remove Cl^-, CH_3COO^-, and SO_4^{2-} salts of Hg^{2+}, Cd^{2+}, and Pb^{2+} with notable adsorption capacity. Other than this, the study has shown correlations between metallogel strengths and their fabrication methods. Herein, the remediation of water by xerogel **G8GE** has been further investigated using ICP-AES, PXRD, BET and XPS techniques.

2. Experimental

2.1 Materials and methods

The chemicals used in this work, *viz*., cyanuric chloride, 5-amino tetrazole monohydrate, 3,4-diaminobenzoic acid, trimesoyl chloride, and heavy metal salts, have been taken from commercial sources. DMSO/MQ–water or a mixture of solvents was used for experimental analysis. Fourier-transform infrared (FTIR) analysis was carried out using a Bruker tensor 27 FTIR spectrophotometer. NMR spectra were obtained using an AVANCE NEO500 Ascend Bruker Biospin International AG at ambient temperature using DMSO-d_6. For ESI-MS (electrospray ionization mass spectrometry) mass data, a Bruker Daltonics micro TOF-QII was used. Morphological study and 3-D transformation from organogels to metallogels have been analysed

using a Supra55 Zeiss field emission scanning electron microscope (FE-SEM). The removal of heavy metal ions from contaminated water has also been confirmed by analysis of the surface area of xerogels, which was carried out using a Quantachrome, Autosorb iQ2 Brunauer–Emmett–Teller (BET) surface area analyser. It was also examined using PXRD, XPS, and ICP-AES techniques.[19,47,48]

2.2 Characterization

To investigate the presence of various functional groups and changes during the formation of organogel and metallogels, FTIR analysis was carried out for gelator molecules **G8** and **GE**, the xerogel of organogel **G8GE**, and metallogels **M1G8GECl$_2$**, **M1G8GE(OAc)$_2$**, **M1G8GESO$_4$**, **M2G8GECl$_2$**, **M3G8GECl$_2$**, **M3G8GE(OAc)$_2$**, where **M1** = Hg(II), **M2** = Cd(II) and **M3** = Pb(II) ions. The values of storage modulus and thixotropic behaviour for organogel and all the metallogels have been determined using a rheometer. The interaction ratio between **G8:GE** and all the studies related to fluorescence data have been recorded with a Fluoromax-4 spectrofluorometer (HORIBA Jobin Yvon, model FM-100) in a quartz cuvette (10 mm × 10 mm). The changes found during the formation of metallogels by mixing and by adsorption have been studied by FE-SEM analysis performed using a Supra55 Zeiss FE-SEM. The powder X-ray diffraction (PXRD) pattern for gelator molecules and all the xerogels have been studied with a Rigaku smart lab automated multifunctional X-ray diffractometer with a Cu Kα source (the X-ray wavelength was 0.154 nm), 2θ range of 5–90°, 0.02° step size, and 3° min^{-1} scan speed. Removal of heavy metal ions from contaminated water, recyclability of **G8GE** towards separation, and water remediation at different pH from acidic to basic, were studied through ICP-AES analysis. The surface area changes during the removal of heavy metal ions have been analysed using BET and XPS analysis.

2.3 Synthesis of gelator components G8 and GE

The gelator molecule **G8** was synthesized using a previously reported method.[46] For the synthesis of **G8**, 2.47 g (24 mmol) of 5-amino tetrazole monohydrate and 3.34 mL (24 mmol) of triethylamine were taken in 80 mL ethanol under ice-cooled conditions, and 8 mmol (1.472 g) of solid cyanuric chloride was added into it by small portions. The reaction mixture was refluxed for 3 h at 80 °C. After the reaction was completed, the precipitate was filtered and washed with 3N HCl, water, and methanol before being dried at room temperature under vacuum (Scheme 1), and the desired gelator molecule **G8** was obtained. Product yield 80%.

The synthesis of organic molecule with carboxamide, amine, and carboxylic acid groups for providing extensive hydrogen bond forming sites to **G8** has been designed, which can strategically enhance the physical and chemical properties of organogel **G8**. For the synthesis of 3,3′,3″-(benzenetricarbonyltris(azanediyl))tris(4-aminobenzoic acid) as a gelation enhancer (**GE**), 1.82 g (12 mmol) of 3,4-diaminobenzoic acid and 1.67 mL (12 mmol) of triethylamine were taken in 50 mL of dry DCM and the mixture was added dropwise into 50 mL chloroform solution of 1.06 g (4 mmol) of trimesoyl chloride under ice-cooled conditions. The reaction mixture was kept under this condition for one hour, and then the mixture was refluxed for 12 hours. After the reaction was completed, the precipitate was filtered and washed with 3N HCl and water before being dried at room temperature under vacuum (Scheme 2). Product: yield: 83%. MS (ESI) of **GE** *m*/*z*: 613 (in positive mode) (Fig. S1, ESI†). ^{1}H NMR (500 MHz, DMSO-d$_6$) δ ppm 10.47 (3 H), 8.68 (9 H), 8.19 (3 H), 7.81 (3 H), 7.61 (3 H), and 6.83 (amide–NH proton) (Fig. S2, ESI†). ^{13}C NMR (126 MHz, DMSO-d$_6$) δ ppm 113.48 (6 C) 116.78 (6 C) 118.81 (3 C) 121.79 (3 C) 132.55 (3 C) 141.09 (3 C) 167.73 (3 C) 168.35 (3 C) (Fig. S3, ESI†). FTIR of **GE**: 1700 cm^{-1}, 1659 cm^{-1}, 1602 cm^{-1}, 1520 cm^{-1}, 1428 cm^{-1}, 1301 cm^{-1}, 1225 cm^{-1} (Fig. S4, ESI†).

2.4 Gels preparation

The synthesized molecule 3,3′,3″-(benzenetricarbonyltris(azanediyl))tris(4-aminobenzoic acid) behaves like a gelation enhancer (**GE**) along with **G8**, which enhanced the strength and stability of the gel even in water in comparison with the previously synthesized gel only out of **G8** (N^2,N^4,N^6-tri(1*H*-tetrazol-5-yl)-1,3,5-triazine-2,4,6-triamine). For the formation of **G8GE** organogel, 0.03 mmol of **G8** and 0.03 mmol of **GE** were solubilised in 1 mL of DMSO by heating. After a clear red-brown solution of **G8GE** was obtained, 1 mL milli Q water was added to it. Instantaneously a yellowish-brown coloured organogel was formed. Similarly, 0.03 mmol of each gelation component (*i.e.*, **G8** and **GE**) was dissolved in 1 mL DMSO by heating, and 0.03 mmol of heavy metal salt dissolved in 1 mL Milli Q water was added separately. After mixing with each other, red brown metallogels of **M1G8GECl$_2$**, **M1G8GE(OAc)$_2$**, **M1G8GESO$_4$**,

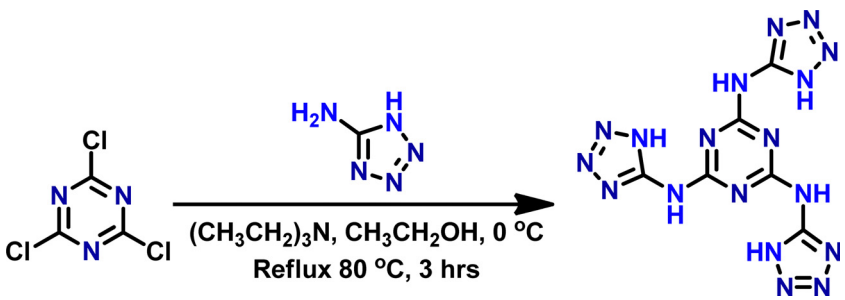

Scheme 1 Synthesis of gelator **G8**.

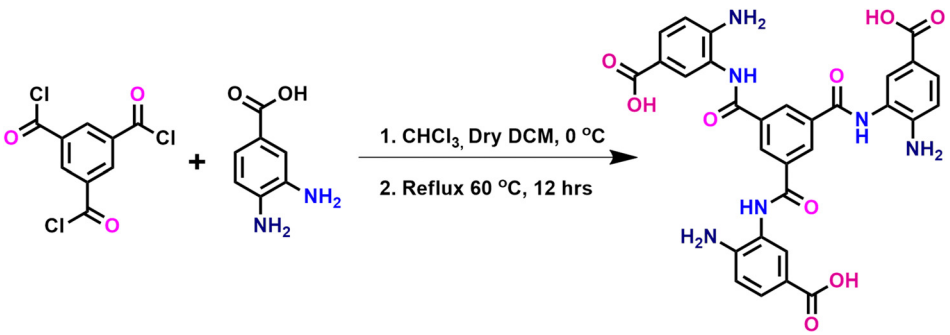

Scheme 2 Synthesis of gelator enhancer **GE**.

M2G8GECl$_2$, **M3G8GECl$_2$**, and **M3G8GE(OAc)$_2$**, were fabricated where **M1** = Hg(II), **M2** = Cd(II) and **M3** = Pb(II). However, using this method, no metallogel formation was observed with Cd(OAc)$_2$ and $CdSO_4$. Similarly, for metallogel formation using the adsorption method, firstly, organogel **G8GE** was fabricated, and then 1 mmol of individual metal salt dissolved in 1 mL milli Q water was slowly added into the upper layer of the organogel of **G8GE**. After 24 hours, the upper aqueous layer was removed and strong metallogels *viz*. **M1G8GECl$_2$Ads**, **M1G8GE(OAc)$_2$Ads**, **M1G8GESO$_4$Ads**, **M2G8GECl$_2$Ads**, **M2G8GE(OAc)$_2$Ads**, **M2G8GESO$_4$Ads**, **M3G8GECl$_2$Ads** and **M3G8GE(OAc)$_2$Ads** were formed. All the gel formation was confirmed using the test tube inversion method, where gels do not flow under the effect of gravitational force.

2.5 Morphology of gels

Morphological studies of organogel **G8GE** and its metallogels with heavy metal salts have been investigated using FE-SEM technology. The SEM images described the changes in self-assembly from organogel to respective metallogels. For this analysis, the sample preparation was carried out on a small glass slide and, after drying, it was coated with a gold 10 mm coating. The coating thickness can be increased or decreased based on the sample nature.

2.6 Rheological properties of gels

Oscillating rheology was performed on an Anton Paar physica MCR 301 rheometer for investigation of the mechanical and thixotropic behaviour of organogels and metallogels. The experiments were carried out with a 25 mm parallel plate with a 0.5 mm true gap at 25 °C. Frequency sweep experiments were completed for the organogel and all the metallogels at 0.5% strain which was taken from the angular sweep experiment of organogel **G8GE**. The strain sweep experiment with time or thixotropic behaviour was tested at minimum 0.5% and maximum 100% strain. For the experiment, direct gel was put on the stage of the rheometer with the help of a spatula with minimum disturbance.

2.7 Gel melting temperature

The melting temperature of the organogel and metallogels was determined with the help of a silicon oil bath. 2 mL v/v gel in DMSO : H_2O was formed in a 5 mL glass vial, and it was immersed in a silicon oil bath on a manual heating plate. When the temperature began to increase, the changes could be seen for the conversion of the gel towards a sol. The temperature at which the gel start getting converted into a sol can be seen using a thermometer, which was dipped in the oil bath. This temperature was noted as the melting temperature or transition temperature of gel (T_{gel}). After complete conversion of the gel into sol, the heating was turned off. After 10 min the sol was again converted into a gel showing the gel–sol–gel transition property of the gel.

3. Results and discussion

Water is an essential part of our life. Contamination of water bodies by various pollutants like heavy metals is a challenging issue, and developing suitable materials to reduce such pollution is receiving attention for researchers worldwide. There are many reports on removing heavy metal contamination from water using nanocomposite powder and other hybrid materials.[49–52] Out of those adsorbents, the new material for water purification as an adsorbent, *i.e.*, gels, is introduced with its great sensitivity toward metal ions and its heterogenous nature within the water system.

In this work, the synthesis of the organic molecule **GE** is strategized as it contains carboxamide, amine, and carboxylic acid sites with the chances of generating extensive hydrogen bonds. For the synthesis of a gelation enhancer (**GE**), diaminobenzoic acid and triethylamine were taken in 50 mL of dry DCM, and the mixture was added dropwise into 50 mL of chloroform solution of trimesoyl chloride under ice-cooled conditions. The reaction mixture was kept under this condition for one hour, and then the mixture was refluxed for 12 hours. After the reaction was completed, the precipitate was filtered and washed with 3N HCl and water before being dried at room temperature under vacuum. **GE** was characterized using ESI-MS, FTIR, ^{1}H, and ^{13}C NMR spectroscopy. The IR spectrum of the **GE** molecule reveals the characteristic band for carboxylic acid C=O at 1700 cm^{-1}, carboxamide C=O at 1659 cm^{-1}, amide N–H at 1602 cm^{-1}, primary amine N–H at 1520 cm^{-1}, and the presence of C–O at 1225 cm^{-1}. In the ^{1}H NMR spectrum, the carboxylic acid proton was observed at 10.47 ppm, aromatic protons were

observed within the range of 8.68–7.61 ppm, and amide –NH proton was found at 6.83 ppm. In ^{13}C NMR, the peak for carboxylic carbon was found at 168.35, for carboxamide carbon at 167.73, and those for all the aromatic carbons were found between 141.09 to 113.48 ppm. The ESI-MS spectrum shows the molecular ion peak at 613 in positive mode, confirming the synthesis of GE.

However, we could not find a suitable solvent composition that can allow **GE** to form a stable gel, albeit a robust one. Therefore, we thought to study the influence of **GE** in the fabrication of gel with the previously synthesized gelator molecule **G8**, which also has many sites for hydrogen bond interaction. It is easily noted that the hydrogen-bond formations could be complementary between **G8** and **GE** (Scheme 3). As expected, the results of the interaction of **G8** with **GE** gave a water-stable organogel **G8GE**. It also shows metallogel fabrication with heavy metal salts by mixing gel components in DMSO : H_2O mixture and metallogels **M1G8GECl_2**, **M1G8GE$(OAc)_2$**, **M1G8GESO_4**, **M2G8GECl_2**, **M3G8GECl_2**, and **M3G8GE$(OAc)_2$** are obtained. Interestingly in these cases, the strength of the gel was found to be decreased with the incorporation of metal ions, which is the reverse of the general trend.[53,54] It signifies that the non-covalent interactions between **G8** and **GE** molecules are disturbed by the insertion of metal salts with mixing. To overcome this disturbance, we have taken the unique approach of allowing the metal ions to diffuse through the bulk gel materials in a layering technique, revealing the increased storage modulus of metallogels compared to the organogel and mixed metallogels. This observation also led to the application of mixed organogels in heavy metal adsorption from aqueous solution. This will open the door to utilizing this untapped technique for water remediation.

3.1 Critical gel concentration, hydrophobic and shape forming nature of organogel G8GE and their metallogel formation with heavy metal salts

In an earlier communication, we reported that **G8** could form a gel with a DMSO and H_2O mixture, but it has also been observed to become soluble in water after sonication. When **G8** and **GE** are dissolved in 1 mL of DMSO and 1 mL H_2O was added into it, rapid gel formation occurs. This gel has been found to be hydrophobic in nature; it was not soluble in water even after sonication or stirring for an extended period. Notably, a very minimum concentration of **G8** and **GE** can also show gel formation. To determine the CGC values of organogel **G8GE**, different amounts of **G8** and **GE** were taken from 0.01 to 0.1 mmol with a constant volume ratio of DMSO : H_2O, taking each solvent in 1 mL of volume. It was found that even 0.01 mmol (3 mg) of **G8** and 0.01 mmol (6 mg) of **GE** in 2 mL of a DMSO : H_2O mixture formed a transparent yellowish-brown gel. Therefore, the CGC for **G8GE** is 10 mM (0.01 mmol per mL) (Fig. 1(a)). Attempts to fabricate a gel with a further lower concentration of **G8** and **GE** were not successful.

The Job plot, for which the fluorescence experiment was done, suggested that the ratio of the interaction of **G8 : GE** is maximum at 3 : 2, so the **G8GE** organogel was fabricated at a 3 : 2 ratio, *i.e.*, with 0.03 and 0.02 mmol, respectively. However, the rheological experiments carried out with organogel **G8GE** in different concentrations starting from 0.01 to 0.1 mmol indicated that the most effective concentration for the strongest gel formation is a 1 : 1 ratio of **G8** and **GE** with 0.03 mmol of each in 2 mL of a DMSO : H_2O mixture (Fig. 1(b)–(d), Fig. S5–S7 and Table S1, ESI†). Previously, organogel **G8** was fabricated and was found to be less stable in water than the mixed organogel **G8GE** reported here. The hydrophobicity of the fabricated gel was checked with the addition of the **G8GE** gel in water in a

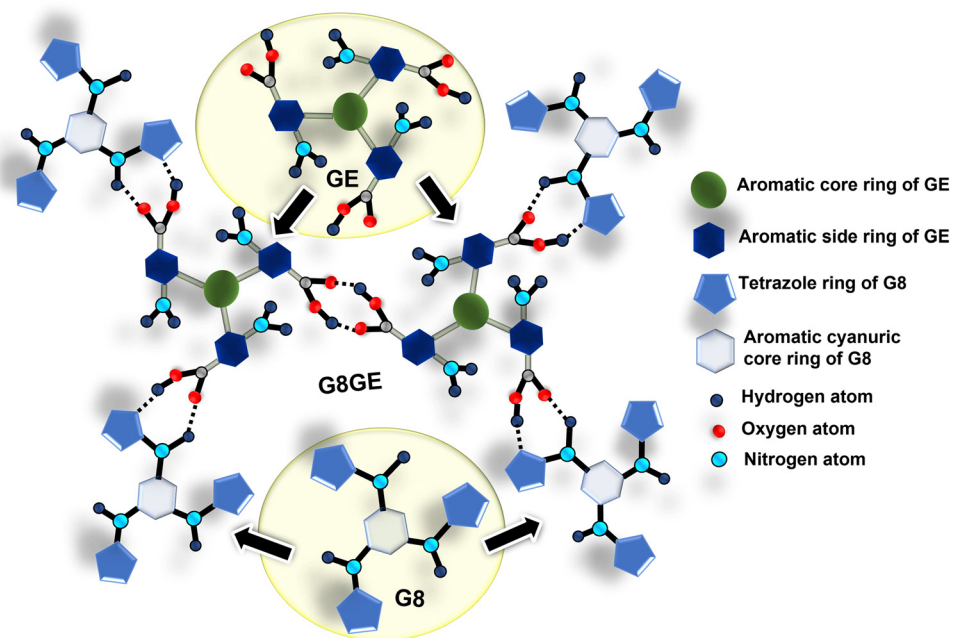

Scheme 3 **G8** and **GE** showing alternative hydrogen bond donor–acceptor sites.

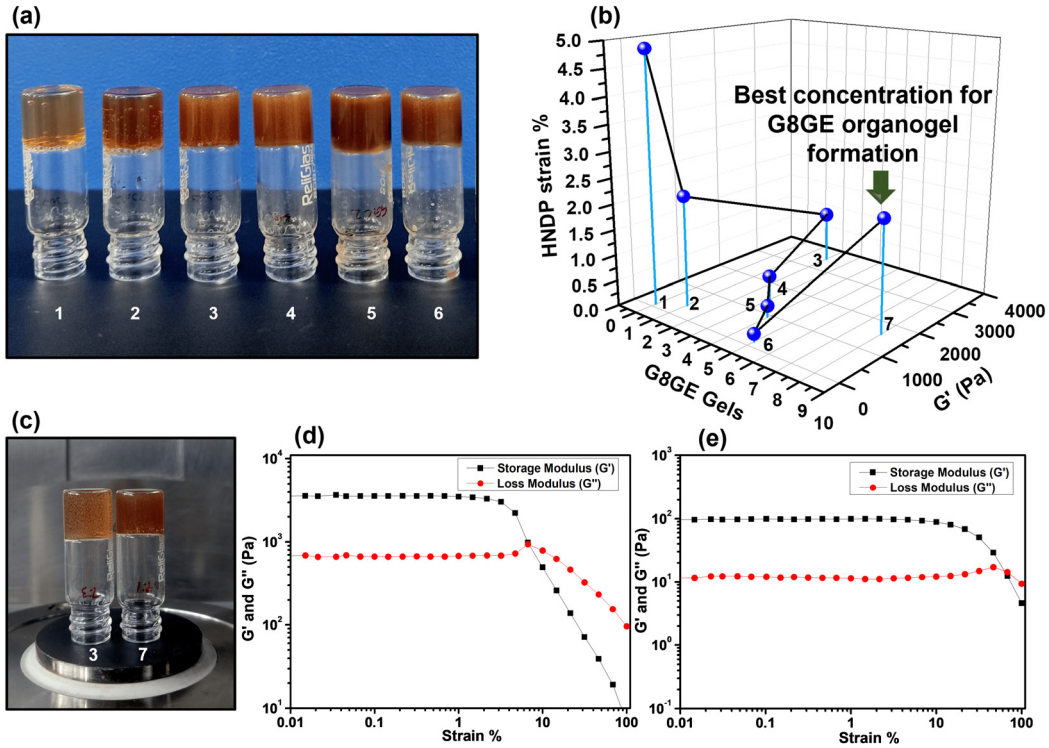

Fig. 1 (a) Formation of gel **G8GE** at different concentrations. (b) 3D graph showing the best gelation concentration for the **G8GE** organogel. (c) Images of organogel **G8GE** at a 1 : 1 and 3 : 2 ratio. (d) Linear viscoelastic (LVE) experiment for **G8GE** under 0.03 : 0.03 mmol conditions. (e) LVE experiment for **G8GE** under 0.03 : 0.02 mmol conditions.

beaker with the help of a syringe, and it was found that the drop of gel formed a flat circular disc-like shape within the water layer. After adding several drops, many such disc-shaped structures can be seen inside the water and separated from each other. Its hydrophobicity was also checked by making a circle with a gel in a petridis containing water. The formed structures within the water layer remain as such, with no apparent change in shape or size, indicating the hydrophobic nature of the gel system. The organogel **G8GE** has a soft, flexible nature, because of which it can be shaped into different structures (Fig. 2(a)–(c)).

The metallogel formation has been explored with **G8GE**, and it was found that with a suitable proportion of gelator components and metal salts, the fabrication of gels can be achieved with $HgCl_2$, $Hg(OAc)_2$, $HgSO_4$, $CdCl_2$, $PbCl_2$ and $Pb(OAc)_2$. However, no gel formation was observed with $Cd(OAc)_2$ and $CdSO_4$; rather, gelatinous solutions were obtained indicating the involvement of the counter-anions as well. Another method has been used to form metallogels, *i.e.*, the adsorption method by which the metallogel fabrication has been carried out with all three heavy metal (Hg, Cd, and Pb) salts. It is fascinating to note that in these cases, the metallogels formed by the adsorption method have shown much higher strength with respect to the metallogels obtained by simple mixing (Fig. 2(d) and (e)).

3.2 Fluorescence behaviour of gelator components, organogel, metallogels and notable difference using the gelation method

The spectroscopic study of **G8**, **GE**, and **G8GE** gives interesting results. The molecule **G8** with a broad UV-Vis peak in solution around 335 nm showed a fluorescence peak at 445 nm with moderate intensity when excited at 350 nm.[46] The UV-Vis data of **GE** also show a broad UV-Vis peak around 328 nm, and at 350 nm excitation, it gives a fluorescence peak at 428 nm in a DMSO : H_2O solvent system. When the UV-Vis analysis was carried out for the gel made from **G8GE**, a broad UV-Vis peak was found at around 330 nm, which shows an emission peak at 431 nm when excited at 350 nm excitation wavelength (Fig. S8, ESI†). The synthesized gelator enhancer **GE** shows moderate fluorescence (emission wavelength 428 nm), which is a little bit stronger than the **G8** molecule (emission wavelength 435 nm) (Fig. S9, ESI†). However, in **G8GE** where the interaction of **G8** and **GE** is taking place, some intramolecular motions are restricted due to the formation of non-covalent interactions between these two gelator components. As a result, the fluorescence is increased. The data were recorded with **G8GE** solution, **G8GE** gel, and metallogels. It was found that the fluorescence intensity was different under different conditions. When 1 mM DMSO : H_2O solution of **G8** (2 mL), **GE** (2 mL) and **G8GE** (1 : 1 mL) was analysed by fluorescence experiment, the relative intensity was found in the order of **G8** < **GE** < **G8GE** with λ_{max} values at 435 nm, 428 nm, and 431 nm, respectively (Fig. 3(a)). While in the same experiment, when carried out only in DMSO, the relative intensity order remains the same while the λ_{max} values change to 432 nm, 409 nm, and 419 nm respectively (Fig. 3(b)). The values of λ_{max} are greater in the case of DMSO : H_2O as compared to only DMSO, which indicates the presence of intramolecular charge transfer (ICT) within the

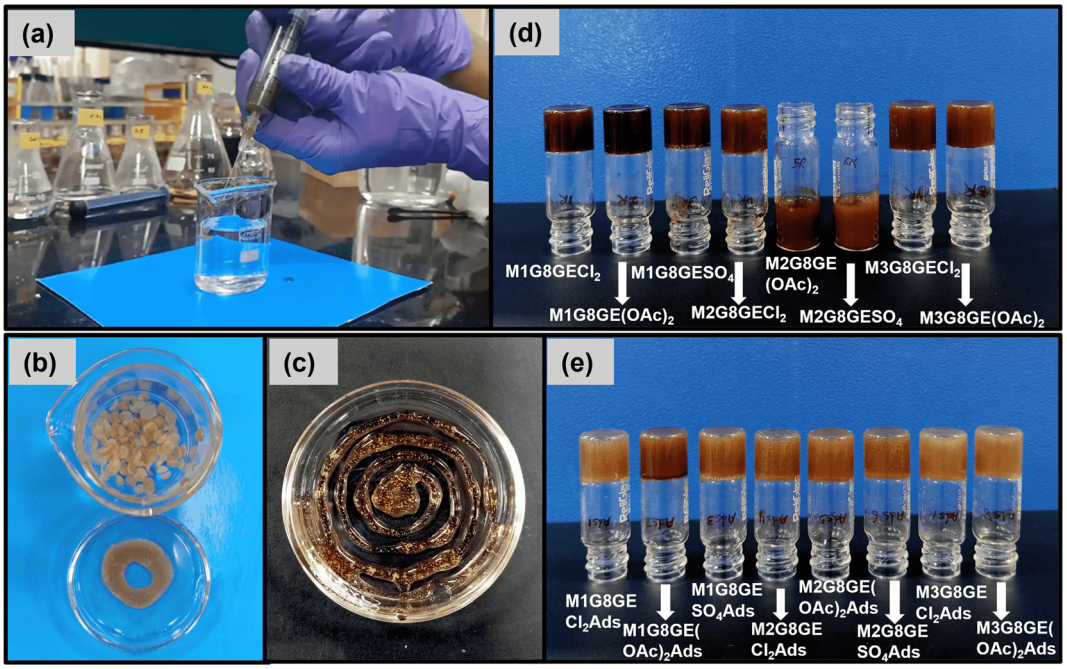

Fig. 2 (a) Addition of organogel **G8GE** in water using a syringe. (b) Image showing the hydrophobic nature of **G8GE** gels in water. (c) Shape formation showing the soft and viscoelastic nature of the gel. (d) Formation of the metallogel of **G8GE** with heavy metal salts by mixing. (e) The formation of the metallogel of **G8GE** with heavy metal salts using the adsorption method.

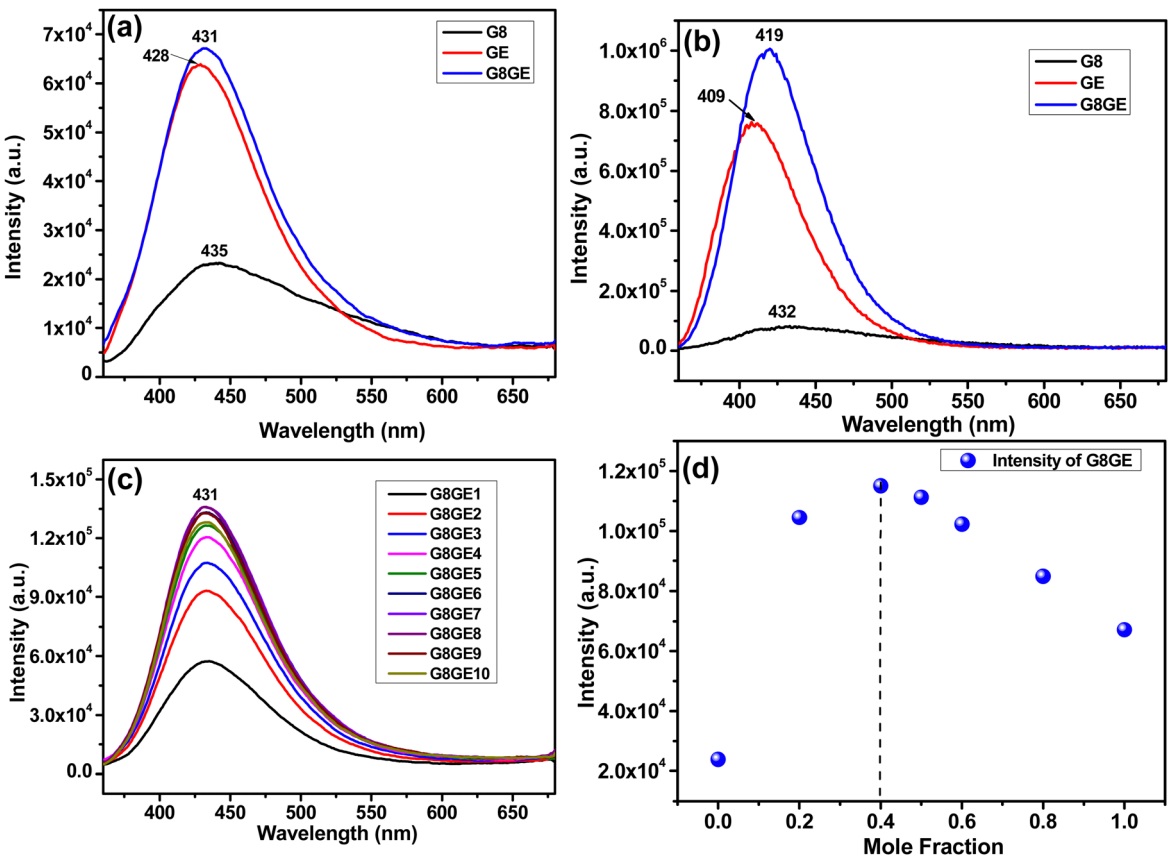

Fig. 3 (a) Fluorescence analysis of **G8**, **GE** and **G8GE** in the DMSO : H_2O mixture. (b) Fluorescence analysis of **G8**, **GE** and **G8GE** in DMSO. (c) AIEE phenomenon for the **G8GE** gelation component. (d) Job's plot showing the ratio of interaction between **G8** and **GE**.

molecules where the wavelength increases with increasing the polarity of the solvent.[55–57] The fluorescence intensity and wavelength were affected by the solvents system, which has been confirmed by fluorescence analysis of 0.3 mM **G8GE** solution in DMSO and in the solvent combinations (1 : 1) of DMSO : EA, DMSO : DMF, DMSO : MeCN, DMSO : MeOH, DMSO : EtOH and DMSO : H_2O. In the case of polar aprotic solvents, the intensity was much higher than polar protic solvents with lower wavelengths of λ_{max} values (Fig. S10, ESI†). The driving force behind this observation might be the hydrogen bond formation in polar protic solvents with **G8** and **GE** gelation components. This led to the disturbances in the interactions of **G8** and **GE**, resulting in the decrement in fluorescence.

The solution of **G8GE** also shows aggregation-induced enhanced emission (AIEE).[58] For this, 1 mM solution of **G8GE** in a DMSO : H_2O mixture was taken as a stock solution, and the fluorescence intensity was found to be increased with increasing concentration. This might be due to the restriction in intermolecular rotation with the aggregation of **G8GE** molecules (Fig. 3(c)). Interaction of **G8** with **GE** by Job plot indicated that the 0.4 mole fraction of **GE** shows a higher fluorescence intensity. Therefore, the interaction ratio for **G8 : GE** is 3 : 2 (Fig. 3(d) and 4(b)).

Fluorescence experiments were also carried out by dissolving organogel and metallogels in DMSO. As a general methodology, 50 mg of gel which was formed by mixing, was dissolved in 3 mL of DMSO, and fluorescence data were recorded with 350 nm excitation. It was found that the intensity of the **G8GE** gel was greater than those of other metallogels, and in the case of **M1G8GE(OAc)$_2$**, it was almost quenched. However, the fluorescence data of metallogels formed by adsorption show increased fluorescence intensities compared to mixed metallogels (Fig. S11a and b, ESI†). The reason might be the disturbances created by the metal insertion in the assembly of **G8GE** molecules during its mixing. However, in the case of adsorption-based gels, metal ions are allowed to take favourable positions within the gel matrix without much disturbance, thus reinforcing the assembled structures making the fluorescence intensities stronger. To understand the influence of Hg(II) on the florescence properties of **G8GE**, 1 mM solution of organogel in DMSO was treated with increasing concentration of Hg(II) by gradual addition of 1 mM solution of $HgCl_2$ in H_2O in a constant volume. With the decreasing amount of **G8GE** and an increasing amount of $HgCl_2$, a significant decrement in fluorescence with a slight bathochromic shift is observed. Similarly, when the same experiment was carried out by dissolving **G8GE** and mercury salt in a 1 : 1 mixture of DMSO and H_2O, a similar observation was recorded (Fig. S12, ESI†). The data indicate that the incorporation of metal ions interferes with the non-covalent bonding between **G8** and **GE**.

3.3 Morphological analysis of the organogel and metallogel of G8GE

The morphology of the **G8** organogel was found to be a continuous tiny fibre-like structure, as reported in our previous

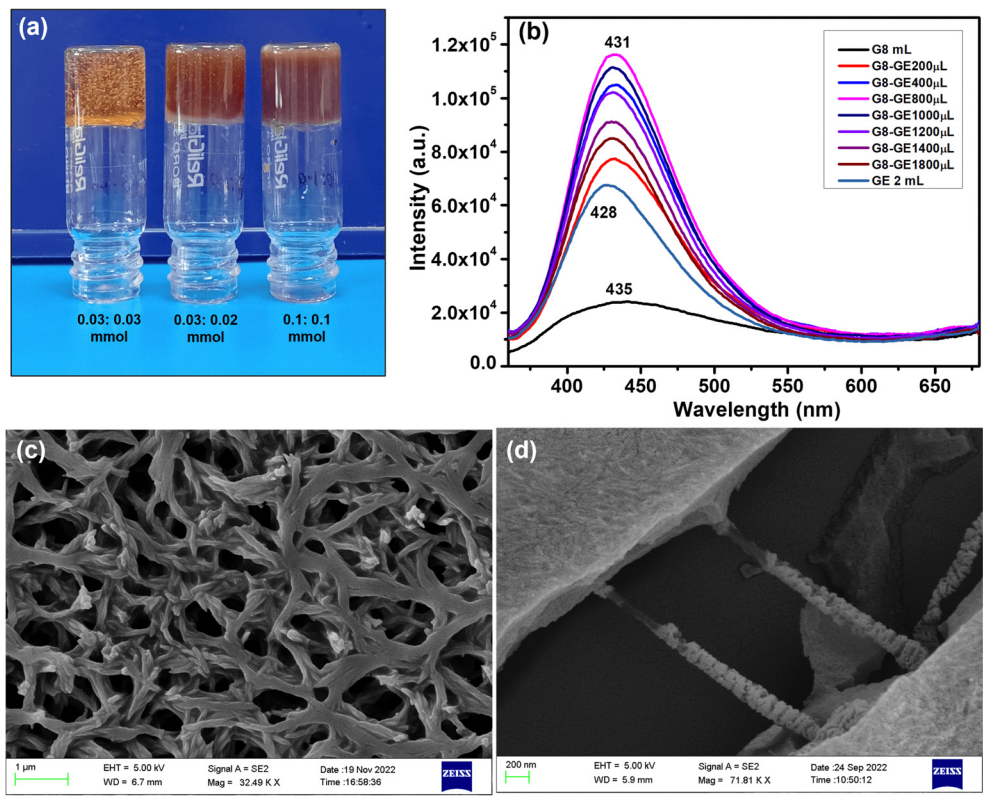

Fig. 4 (a) Organogel **G8GE** at different concentrations. (b) Ratio of interaction of **G8** and **GE**. (c) FE-SEM image of **G8GE** (gel of 0.03 : 0.03 mmol of **G8** and **GE**) and (d) FE-SEM image of **G8GE** (gel of 0.1 : 0.1 mmol of **G8** and **GE**).

work.[46] When the **G8** molecules were combined with **GE**, a drastic change was observed in the morphology. Interestingly, morphology changes were also observed with **G8** and **GE** ratio alteration. When the gel is formed with 0.03 mmol of each of **G8** and **GE** in 2 mL of DMSO–H_2O solution, the morphology reveals nano-branched thread-like structures connecting to make a net of gel fibers. However, in higher concentrations with 0.1 mmol of each of **G8** and **GE**, it shows nano thread-like structures which are closely packed within the 3D network of the gel. These indicate that branches in higher concentrations of gel are closely packed to cover a wider area as connected with nano-threads (Fig. 4). These 3D changes in morphology from organogel **G8** (continuous tiny fibre-like structure) to mixed organogel **G8GE** (nano-branched threads) reveal that the self-assembly of **G8GE** forms a more robust gel network.

Furthermore, the formation of metallogels of **G8GE** with heavy metal salts also shows 3D nanostructured metallogel fabrication. The FE-SEM images confirmed that the metallogel morphologies are different when fabricated following different methods, *i.e.*, mixing and adsorption methods. The mixing method furnished metallogel **M1G8GECl$_2$** with a sharp leaf and flower pattern, **M1G8GE(OAc)$_2$** with flower-like morphology, **M1G8GESO$_4$** and **M2G8GECl$_2$** with a network structure of threads. A leaf-like closely packed structure attached to each other was obtained for **M2G8GE(OAc)$_2$** while in **M2G8GESO$_4$**, **M3G8GECl$_2$** and **M3G8GE(OAc)$_2$** dense fibrous morphology is recorded (Fig. 5). The metallogel fabricated using adsorption methods shows dense fibrous morphology for all the cases. This signifies that with this method, metal ions do not disturb the **G8GE** gel matrix significantly (Fig. S13, ESI†). EDX and mapping analysis has been carried out and found the presence of respective elements inside the gel matrix (Fig. S14–S21, ESI†).

3.4 Effect of the method of gel formation on their rheological properties

A rheological study was taken up to determine the relative gel strength. A significant difference was found between the gel strength of previously fabricated organogel **G8** and the modified organogel **G8GE**. The value of storage modulus (G') for **G8** was 236 Pa[46] while the value for **G8GE** (0.03 : 0.03 mmol, 1 : 1 ratio) is 3517 Pa and 1593 Pa for 3 : 2 (0.03 : 0.02 mmol) of **G8** : **GE** (Fig. S22, ESI†). When metallogels were formed by the mixing method, the values of storage modulus (G') for **M1G8GECl$_2$**, **M1G8GE(OAc)$_2$**, **M1G8GESO$_4$**, **M2G8GECl$_2$**, **M3G8GECl$_2$** and **M3G8GE(OAc)$_2$** were found to be 1976, 189, 4838, 176, 140 and 2646 Pa respectively indicating the role of counter anions in the gel strength (Fig. S23–S28 and Table S2, ESI†). While gel formation was achieved using an adsorption method, the values of storage modulus for **M1G8GECl$_2$Ads**, **M1G8GE(OAc)$_2$Ads**, **M1G8GESO$_4$Ads**, **M2G8GECl$_2$Ads**, **M2G8GE(OAc)$_2$Ads**, **M2G8GESO$_4$Ads**, **M3G8GECl$_2$** and **M3G8GE(OAc)$_2$** were found to be 11 730, 3055, 10 872, 11 830, 13 815, 13 635, 10 747 and 13 119 Pa respectively (Fig. S29–S36 and Table S3, ESI†). This indicates that the adsorption method provides stronger metallogels with respect to the mixing method. This might be due to some disturbances in the assembled structure between the gelator components **G8** and **GE**, while metal ions are incorporated through mixing (Fig. 6). However, the adsorption method allows the metal ions to diffuse through the gel network without any disturbance to take up the preferred positions inducing a more robust gel fabrication.

3.5 Study on the self-assembly of G8GE gelator components and their gels

Based on the Job plot, which was analysed using a fluorescence method, the ratio of maximum interaction between **G8** and **GE** was found to be 3 : 2. An organogel was formed with this ratio, and the IR data of the xerogel revealed that the carboxylic acid group, tetrazole –NH and secondary amine of **G8** and **GE** participate in the formation of hydrogen bonds providing a strong gel network of **G8GE**. It was already reported that the gelator molecule **G8** shows the IR band at 1339 cm^{-1} for the presence of the cyclic –C–N=C– group, at 1523 and 1422 cm^{-1} for tetrazole. The presence of a secondary –NH group was

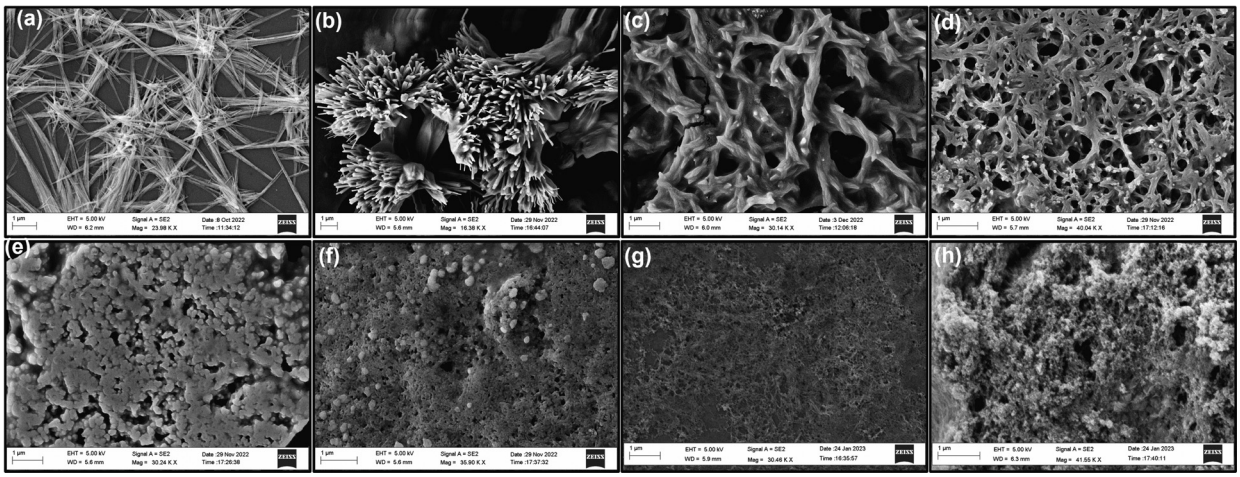

Fig. 5 FE-SEM images of (a) **M1G8GECl$_2$**, (b) **M1G8GE(OAc)$_2$**, (c) **M1G8GESO$_4$**, (d) **M2G8GECl$_2$**, (e) gelatinous solution of **M2G8GE(OAc)$_2$**, (f) gelatinous solution of **M2G8GESO$_4$**, (g) **M3G8GECl$_2$**, and (h) **M3G8GE(OAc)$_2$**.

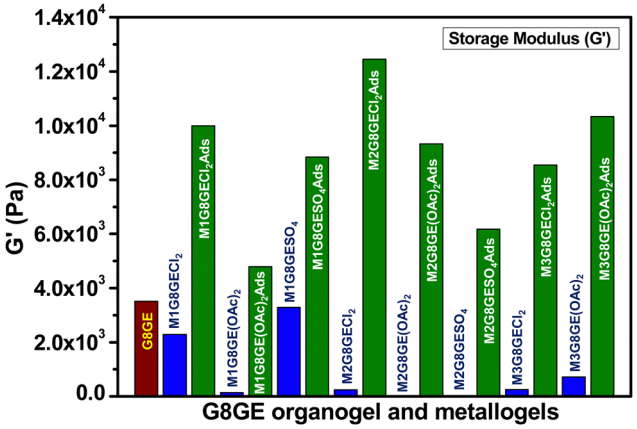

Fig. 6 Comparative study of the value of storage modulus (*G'*) of all the metallogels formed by mixing and adsorption methods.

verified with the band at 1637 cm^{-1}. The gelator component **GE** shows an IR band at 1225 cm^{-1} for C–O, 1520 cm^{-1} for primary amine, 1602 cm^{-1} for amide –NH, 1659 cm^{-1} for amide –C═O and 1700 cm^{-1} for carboxylic –C═O groups. Now, in the case of the **G8GE** xerogel, the IR band of amide –C═O was observed at 1640 cm^{-1} in the place of 1659 cm^{-1}, and the carboxylic acid group shows a broad feature at 1693 cm^{-1}. Also, the IR band at 1422 for tetrazole C–N shifted toward 1415 cm^{-1}. The downward shifts in wavenumbers of these groups strongly recommend their involvement in hydrogen bond formation between **G8** and **GE** (Fig. 7(a)). The fabrication of gels was also studied using a PXRD technique. In the case of **G8** peaks observed with the value of $2\theta = 20.12^\circ$ (d = 4.48 Å) for intercolumnar stacking, $2\theta = 27.64^\circ$ (d = 3.32 Å) for π–π stacking and $2\theta = 34.35^\circ$ (d = 2.73 Å) for hydrogen bonding while for **GE** peaks are at $2\theta = 25.52^\circ$ (d = 3.57 Å) and $2\theta = 42.39^\circ$ (d = 2.28 Å) for π–π stacking and hydrogen bonding respectively. When the organogel **G8GE** was formed, the PXRD peaks found at $2\theta = 21.30^\circ$ (d = 4.24 Å) indicated the presence of intercolumnar stacking, $2\theta = 25.66^\circ$ (d = 3.56 Å) and $2\theta = 27.50^\circ$ (d = 3.33 Å) shows the presence of π–π stacking between **G8** and **GE**.[59–61] The PXRD pattern of **G8**, **GE**, and **G8GE** shows that these are crystalline in nature (Fig. 7(b)). On the basis of the interaction ratio between **G8** and **GE** *i.e.*, 3 : 2 and downward shifting in the IR band of carboxylic acid, secondary amine, and tetrazole nitrogen, a plausible structure with probable hydrogen bonding interaction was proposed for the organogel **G8GE** (Fig. 7(c)).

To confirm the probability of the given structure a DFT study was carried out. The stable ground-state geometries of **GE** and **G8** were obtained using the hybrid density functional – B3LYP-D3[62,63] in combination with the 6-31G(d) basis set. The true minimum was confirmed based on the absence of imaginary frequencies. The binding of **GE** and **G8** was studied by optimizing the complex, and the binding energy was computed using the following equation:

$$\text{Binding energy} = E_{\text{Complex}} - (2E_{\text{GE}} + 2 \times E_{\text{G8}})\ldots\text{For structure G8GE}$$

where E_{Complex}, E_{GE} and E_{G8} are the energies of the **GE-G8** complex, **GE** and **G8**, respectively. All calculations were performed using the polarizable continuum model (PCM) with water as the solvent as incorporated in the Gaussian 16 program package. To estimate the strength of hydrogen bonding in the composite gel, the H-bond binding energy (HBE) was calculated based on the bond critical points (BCP of type [3, −1]) according to Bader's atoms in molecules (AIM) theory using Multiwfn.[64] The HBE was estimated using the following equation:[65]

$$\text{HBE} = -223.08 \times \rho(r_{\text{BCP}}) + 0.7423$$

where HBE is in kcal mol^{-1}, and $\rho(r_{\text{BCP}})$ is in atomic units (a.u.).

The binding of **GE** with **G8** (with two molecules of **G8** and two molecules of **GE**) leads to a stabilization energy of ~60 kcal mol^{-1}. The stabilization is largely due to multiple

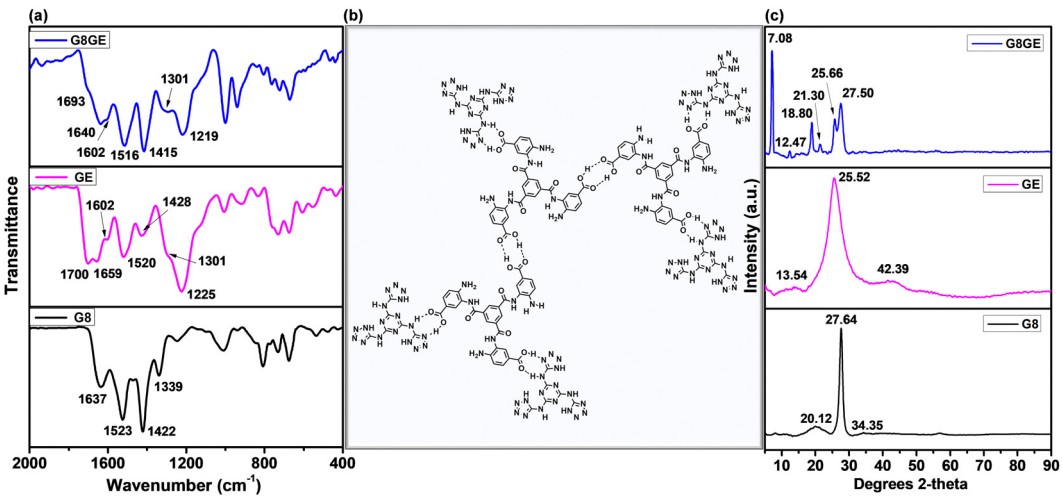

Fig. 7 (a) FTIR data of **G8**, **GE** and **G8GE** xerogels. (b) Possible structure of gelator components **G8GE** interaction. (c) PXRD data of **G8**, **GE** and **G8GE** xerogels.

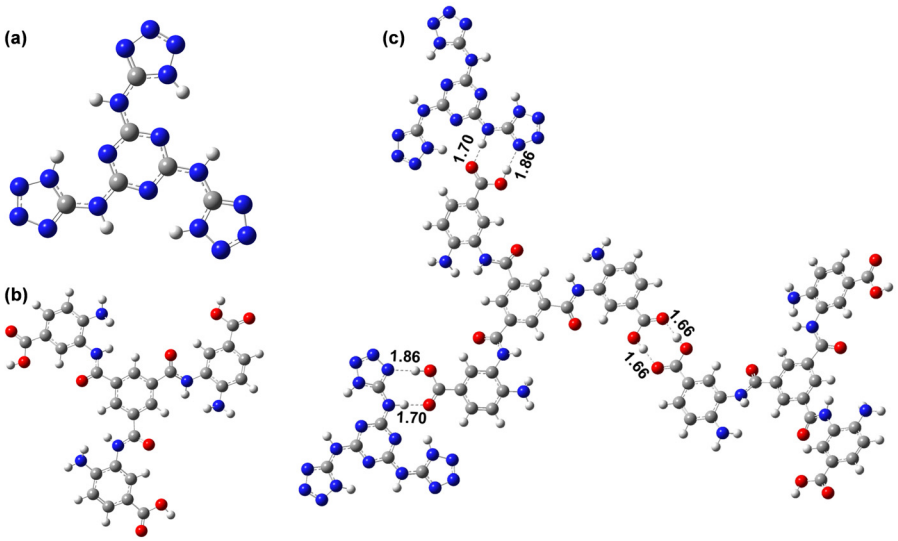

Fig. 8 (a) DFT structure of (a) **G8** and (b) **GE**, and (c) a plausible structure of the interaction of **G8** and **GE**.

intermolecular hydrogen bonds between N–H···O, O–H···N, and O–H···O (Fig. 8). We estimate an average intermolecular hydrogen bond strength of ~ -9.14 kcal mol^{-1} (the hydrogen bond energy per site is provided in Table S10 (ESI†)), Cartesian coordinates of **G8**, **GE**, and **G8GE** (in Tables S11–S13, ESI†) and strong hydrogen bonds in the range of 1.66–1.86 Å. The structures of **G8**, **GE**, and **G8GE** are also shown by DFT (Fig. S37, ESI†). The HOMO–LUMO energy orbitals for **G8** and **GE** are mentioned in the ESI† (Fig. S38).

FTIR analysis of the xerogels of all the metallogels was carried out and the changes in carboxylic, amide, and amine groups were determined, which shows the changes in non-covalent interaction inside the gel system by the insertion of metal ions (Fig. S39, ESI†). To determine the effect of metal insertion on noncovalent interactions in a gel matrix, PXRD data analysis was carried out. All the xerogels of metallogels formed by mixing and adsorption methods show basically three PXRD peaks in the range of 20–23° for intercolumnar stacking, 26–28° for π–π stacking, and 32–45° for hydrogen bonding interactions. The PXRD patterns of all the metallogels are almost the same, showing similar interactions of heavy metal ions with the gelator system **G8GE** (Fig. S40 and S41, ESI†).

3.6 Remediation of water (contaminated water treatment)

The organogel **G8GE** was found to be hydrophobic in nature. It does not get dissolved in water even after sonication of the organogel inside the large quantity of water (*i.e.*, 2 mL gel by volume in around 20 mL of water). The organogel can show shape-forming properties even inside water. After sonication, the organogel is dispersed in water, and it remains as a separated layer of gel inside the mixture. The hydrophobic nature of the gel and the ability to capture metal ions to fabricate metallogels open the route of applying the organogel for capturing toxic heavy metal ions in the remediation process of water. The optimization condition for the removal of heavy metal salt has been analysed with $Hg(OAc)_2$ (1 mM, 20 mL H_2O) with changes in the amount of adsorbent (xerogel) and time of removal reaction (Table S4, ESI†). Optimization shows the best condition for the removal reaction for 1 mM heavy metal salt in 20 mL water was six hours of stirring with 40 mg of xerogel which results in almost 99% removal. Therefore, for the separation of heavy metal ions from water, 20 mL, 1 mM solutions of different metal salts were taken separately and treated with 40 mg of the xerogel of **G8GE**. The solution was kept under stirring at room temperature for six hours. After that, the solutions were filtered, and the filtrates were checked with inductively coupled plasma atomic emission spectroscopy (ICP-AES) to analyse the remaining amount of metal ions in the aqueous system. It was found that xerogel **G8GE** adsorbs 56.27% of mercury chloride, 99.24% of mercury acetate, 99.90% of mercury sulphate, 51.83% of cadmium chloride, 98.68% cadmium acetate, 84.47% of cadmium sulphate, 59.70% of lead chloride and 99.90% of lead acetate from heavy metal contaminated water (Fig. 9). The adsorption capacities (q_e) of the **G8GE** xerogel for different heavy metal salts are given in Table S5 (ESI†). The results show that xerogel **G8GE** adsorbed metal acetate and metal sulphate salts more as compared to metal chloride salt. The reason behind this might be the stronger hydrogen bonding of acetate and sulphate ions with **G8GE** molecules. The more electronegative oxygen atom of acetate and sulphate ion must act as a stronger hydrogen bond acceptor with hydrogen atoms of the primary amine of **G8GE**, while chloride might form a less strong hydrogen bond due to its comparatively less electronegativity. All the experiments and results indicate that the xerogel of organogel **G8GE** is a water remediation material for heavy metal removal from aqueous solution. There are very few reports where gel materials are utilized for capturing heavy metal ions from aqueous solutions. Among them, the current system shows significant efficiency, and the data are presented in Table S6 (ESI†).

After mercury adsorption by xerogel **G8GE**, it can be activated and recycled further. For this purpose, $Hg(OAc)_2$ treated

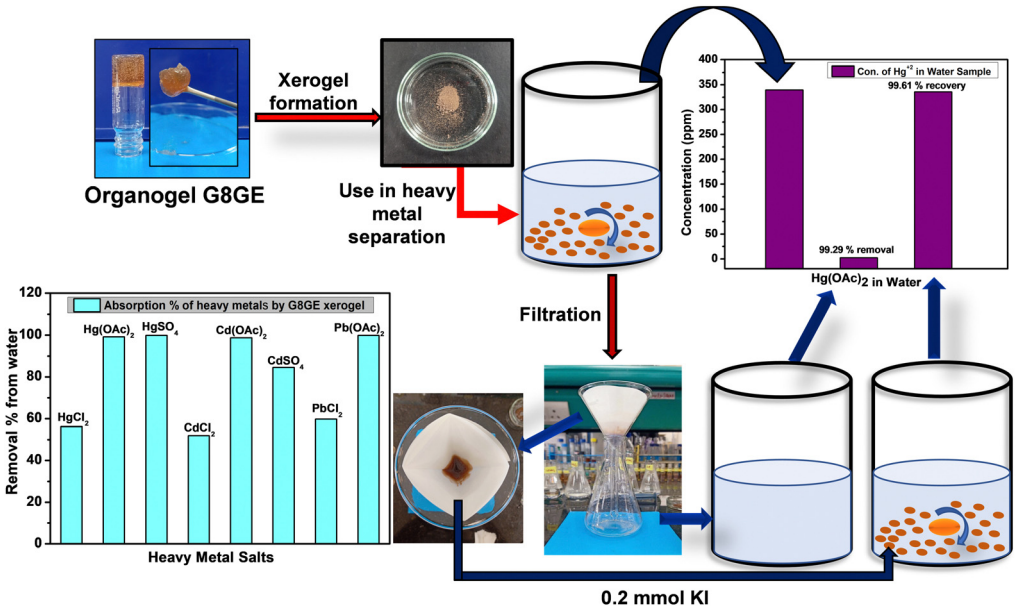

Fig. 9 Systematic representation of the removal of heavy metal salts from contaminated water and their ICP-AES analysis.

xerogel **G8GE** was taken in 20 mL of water, and a small amount of KI (0.2 mmol, 34 mg) was added to it. The mixture was stirred for three hours at room temperature and then filtered. The filtrate was found to contain 99.61% of mercury which was captured within the xerogel during the remediation of water by xerogel **G8GE**. This means only 0.39% mercury could not be recovered from the xerogel **G8GE**. This recovery was analysed by ICP-AES analysis. The activated xerogel was further used successfully for another cycle of heavy metal removal. This regeneration method of adsorbent, *i.e.*, xerogel **G8GE** is a cost-effective method where only by using potassium iodide, which is a common laboratory salt, could the recovery of adsorbent **G8GE** be achieved. Further changes between the fabricated xerogel and the treated xerogel after the recovery of mercury were analysed using a BET technique. BET experiments were performed with N_2 adsorption–desorption analysis at 80 °C and 8 hours degassing time. The BET multipoint surface area for the **G8GE** xerogel before use in heavy metal removal is 6.651 $m^2\ g^{-1}$. After the treatment with $Hg(OAc)_2$ the multipoint BET is found to be 4.010 $m^2\ g^{-1}$ which is less than the original due to the presence of mercury inside the gel matrix. However, after the recovery of mercury from xerogel **G8GE** by treatment with KI, this value was found to be 6.549 $m^2\ g^{-1}$. These changes in multipoint BET clearly indicate the adsorption and removal of mercury from water by xerogel **G8GE** (Fig. S42, ESI†).

The removal of heavy metal salts by xerogel **G8GE** was further examined through XPS analysis. For this, XPS analysis was carried out for xerogel **G8GE**, mercury-treated **G8GE** (**mtG8GE**), and mercury-recovered **G8GE** (**mrG8GE**). The XPS survey spectrum of **G8GE** shows the presence of C1s, N1s, and O1s at 285, 399, and 533 eV, respectively. Similarly, in **mtG8GE**, the peaks at 285, 399, and 533 eV indicated the presence of C1s, N1s, and O1s, respectively, with the addition of two new peaks at 100.9 and 104 eV for Hg $4f_{7/2}$ and Hg $4f_{5/2}$, respectively. Furthermore, the survey spectrum of **mrG8GE** shows similar peaks for C1s, N1s, and O1s with small intensity peaks at 101 and 104 eV for Hg 4f, which indicates that a small amount of Hg remains inside the **G8GE** system (Fig. 10). The C1s spectrum of xerogel **G8GE** reveals peaks at 284.4, 285.2, 287.9, and 288.9 eV for C═C/C–C, C–N/C–O, N–C═N and –COOH/C═O respectively. N1s shows the XPS peaks at 398.8, 399.8, 400.6, and 402.0 eV for $–NH_2$, –C═N, C–NH–C, and –NH, respectively. The O1s spectrum shows the peaks at 530.9, 531.5, and 532.9 eV for the –C–OH, –C═O, and –COOH groups, respectively.[66–71] The XPS analysis of **G8GE**, **mtG8GE**, and **mrG8GE** is outlined in Fig. S43–S45 and Table S7 (ESI†).

The effect on the morphology of the gel after utilization for mercury capture from aqueous solution was also investigated by FE-SEM image analysis (Fig. S46, ESI†). The microscopy reveals a circular shaped morphology comprised of a nanofibrous network. It is quite evident that after capturing mercury when treated with an aqueous solution, the original morphology is altered due to the interactions of the metal ion with the gel network.

3.7 Reusability of xerogels and the effect of pH on the removal of heavy metal ions

To check the reusability of xerogel **G8GE** as a water remediation material, **G8GE** was used for five consecutive cycles to remove mercury, and the removal percentages are recorded as 99.21, 98.39, 98.34, 98.11, and 97.39 from the first to fifth cycle. At the end of every cycle, the used xerogel **G8GE** was recovered by its treatment with KI to remove the adsorbed amount of mercury. These experiments show the reusability of xerogel, where the removal percentages are found to be in the range of 97 to 99% (Table S8, ESI†). The heavy metal separation capability of **G8GE** has been checked in four different pH values of 3, 5.4 (DI water), 7, and 10. The results indicate 72.36, 99.24, 97.69,

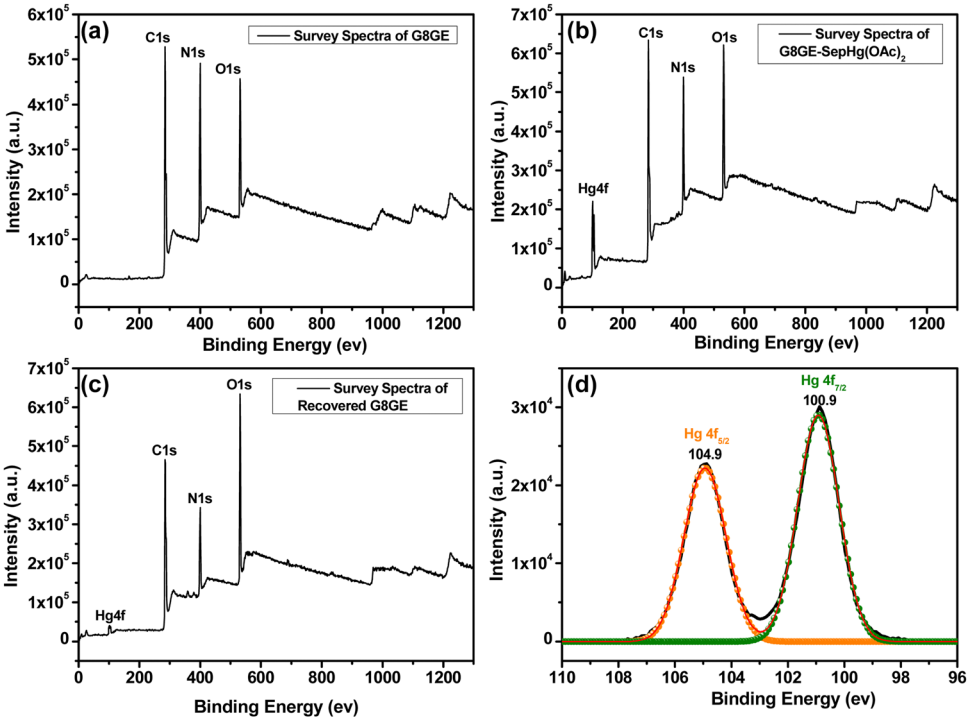

Fig. 10 XPS survey spectra of (a) xerogel **G8GE**, (b) **mtG8GE**, (c) **mrG8GE**, and (d) XPS spectrum of **mtG8GE** showing the presence of Hg 4f.

and 98.26 percent removal of mercuric acetate from aqueous solution (Fig. 11 and Table S9, ESI†).

3.8 Thixotropic modification of metallogels using the adsorption method

The self-healing properties and the thixotropic behaviour of low molecular weight gels aid in the gel–sol–gel transition for many cycles. Organogel **G8GE** also shows good self-healable properties. The time oscillation sweep (TOS) experiment has carried out with three concentrations of organogel at 0.02 : 0.02, 0.03 : 0.03, and 0.04 : 0.04 mmol of **G8 : GE** and it was found that in the case of 0.03 : 0.03 mmol of **G8 : GE** the recovery of storage modulus is continuous and unaffected (Fig. S47, ESI†). The metallogels, which have been fabricated by mixing, show low capacities as thixotropic gels, but metallogels which have been fabricated by the adsorption method, displayed a much better thixotropic nature. More significant decrement of G' values after the first cycle of TOS was observed in the cases of **M1G8GECl$_2$**, **M1G8GE(OAc)$_2$**, **M1G8GESO$_4$**, and **M3G8GE(OAc)$_2$**. It has been reported that within similar gel systems, when the value of G' increases, thixotropic behaviour decreases because of the less viscous nature of gels. However, in this case, when the metallogels have been formed by the adsorption method, the thixotropic nature increases. This is because, during adsorption, the metal ions interact with gelator components without making any disturbance within the **G8GE** gel network. This leads to the viscous nature of the gel being unaffected and is therefore maintained (Fig. 12 and Fig. S48–S51, ESI†).

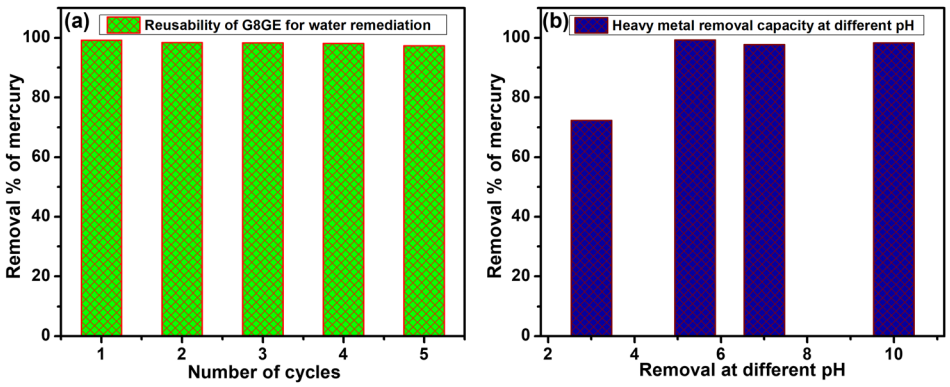

Fig. 11 (a) Reusability of **G8GE** for water remediation. (b) Heavy metal removal at different pH from 3–10.

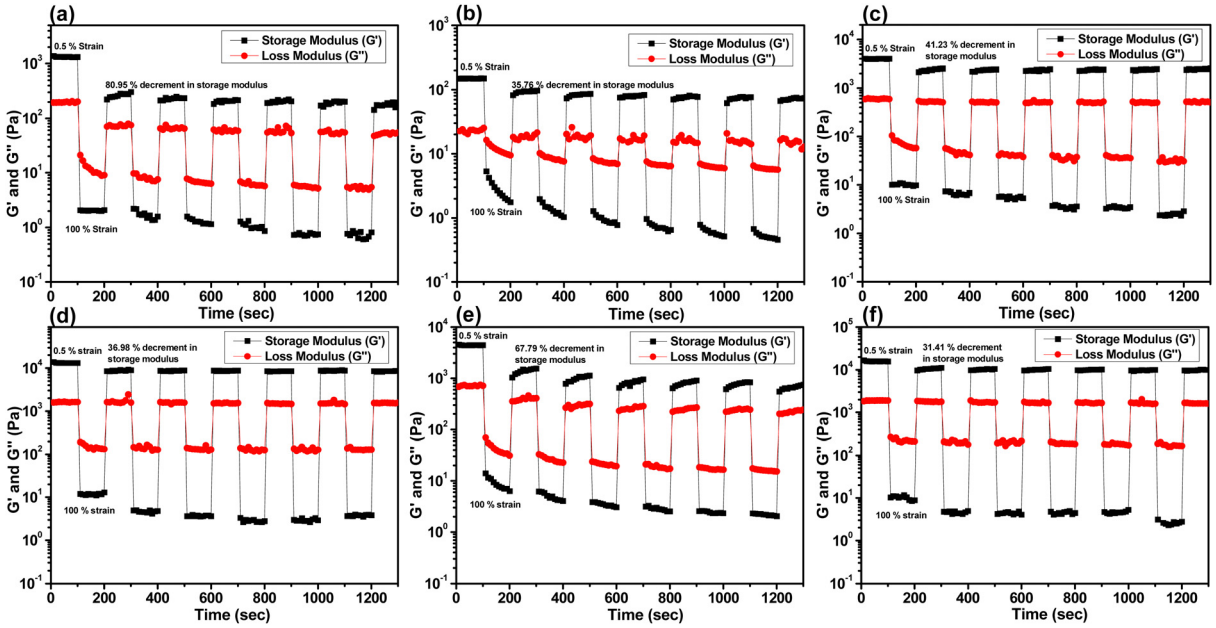

Fig. 12 Comparison of the thixotropic behaviour by time oscillation sweep experiments for metallogels. (a) **M1G8GECl$_2$**, (b) **M1G8GE(OAc)$_2$**, (c) **M1G8GESO$_4$**, and metallogels (d) **M1G8GECl$_2$Ads**, (e) **M1G8GE(OAc)$_2$Ads** and (f) **M1G8GESO$_4$Ads**.

4. Conclusion

This work was focused on utilizing N^2,N^4,N^6-tri(1*H*-tetrazol-5-yl)-1,3,5-triazine-2,4,6-triamine (**G8**), an LMWG, as a prospective heavy metal adsorbing material for water remediation. In a previous report, we observed that **G8** is not stable while treating with excess water, thus is unsuitable for water remediation. Herein, we have developed another organic molecule *viz.* 3,3′,3″-(benzenetricarbonyltris(azanediyl))tris(4-aminobenzoic acid) (**GE**) with complementary hydrogen bond donor–acceptor sites with respect to **G8** as the gel strength enhancer to impart stability even in aqueous medium. The resultant organogel **G8GE** has shown the ability to form metallogels with Hg(II), Cd(II), and Pb(II) salts. The hydrophobicity of the gel was evident from the retention of the disc-shaped gel structure in aqueous medium over a long period of time. With these hydrophobic and metal adsorption properties, mixed organogel **G8GE** has been found to efficiently remove toxic heavy metal salts $HgCl_2$, $Hg(OAc)_2$, $HgSO_4$, $CdCl_2$, $Cd(OAc)_2$, $CdSO_4$, $PbCl_2$ and $Pb(OAc)_2$ from aqueous solution with an effective adsorption capacity (q_e) of 76.24, 157.79, 147.81, 52.09, 131.25, 284.93, 83 and 221.02 mg g^{-1} respectively. The adsorbent xerogel **G8GE** can be recycled for further utilization for five cycles with almost 99% recovery, which was tested for Hg(II) by treatment with KI.

Other than the use of **G8GE** for water remediation, the effect of the method of gel formation on the rheological and fluorescence properties of the gel has also been described here. From the Job's plot, the maximum interactions between **G8** and **GE** were found to be 3 : 2; however, the rheological experiment indicates the fabrication of the strongest gel at a 1 : 1 ratio. Two different methods have been applied for metallogel formation *viz.*, mixing and adsorption method. The fluorescence spectrum of **G8GE** has shown a stronger fluorescence peak with respect to **G8** and **GE** due to the extended non-covalent interactions and, consequently, the reduction in the non-radiative decay process. At lower concentrations, **G8GE** has shown nano-branched thread-like structures in SEM. However, at higher concentrations, a closely packed 3D network of gel is fabricated. Several experiments, including fluorescence properties, morphology determination, and rheological studies, indicated that the adsorption method for the fabrication of metallogels does not disturb the **G8GE** network significantly, while metal ions diffuse through the gel network. Thus, it has been proven to be a more efficient process for gel formation over the mixing method. The DFT optimization study supported the complementary hydrogen bond formation hypothesis between **G8** and **GE**. The limitation of this work is that the adsorption capacities are different with different salts of Hg(II), Cd(II), and Pb(II), which have to be analyzed further. Also, the effect of different metal ions which might be present in contaminated water, for example Hg(II), Cd(II), and Pb(II), in the adsorption process needs to be found.

Conclusively, a hydrophobic organogel **G8GE** has been fabricated with a tendency to form strong metallogels using the adsorption method with heavy metal salts of mercury, cadmium, and lead. This property of mixed organogel makes it suitable for water remediation resulting in the notable adsorption capacity of the **G8GE** xerogel toward heavy metals. This idea of using a gel strength enhancer for different applications of gel materials might create new possibilities in the near future.

Conflicts of interest

There are no conflicts of interest to declare.

Acknowledgements

Reena thankfully acknowledges her PhD fellowship obtained from CSIR (09/1022(0055)/2018-EMR-I). Ritika acknowledges her PhD fellowship obtained from UGC (201610178796). The authors are grateful to SAIF IIT Bombay for ICP-AES analysis and SAPTARSHI IIT Jammu for XPS analysis. The authors are grateful for all the experimental facilities provided by SIC IIT Indore and DST-FIST for the 500 MHz NMR facility.

References

1 H. Wu, J. Zheng, A. L. Kjøniksen, W. Wang, Y. Zhang and J. Ma, *Adv. Mater.*, 2019, **31**, 1806204.
2 N. Malviya, C. Sonkar, R. Ganguly, D. Bhattacherjee, K. P. Bhabak and S. Mukhopadhyay, *ACS Appl. Mater. Interfaces*, 2019, **11**, 47606–47618.
3 N. Malviya, R. Ranjan, C. Sonkar, S. M. Mobin and S. Mukhopadhyay, *ACS Appl. Nano Mater.*, 2019, **2**, 8005–8015.
4 M. He, J. Li, S. Tan, R. Wang and Y. Zhang, *J. Am. Chem. Soc.*, 2013, **135**, 18718–18721.
5 J. H. Lee, H. Lee, S. Seo, J. Jaworski, M. L. Seo, S. Kang, J. Y. Lee and J. H. Jung, *New J. Chem.*, 2011, **35**, 1054–1059.
6 J. R. Xavier, T. Thakur, P. Desai, M. K. Jaiswal, N. Sears, E. Cosgriff-Hernandez, R. Kaunas and A. K. Gaharwar, *ACS Nano*, 2015, **9**, 3109–3118.
7 T. Zhao, G. Wang, D. Hao, L. Chen, K. Liu and M. Liu, *Adv. Funct. Mater.*, 2018, **28**, 1800793.
8 Y. Yang, W. Liu, Q. Zhong, J. Zhang, B. Yao, X. Lian and H. Niu, *ACS Appl. Nano Mater.*, 2021, **4**, 4735–4745.
9 S. G. Roy, A. Kumar, N. Misra and K. Ghosh, *Mater. Adv.*, 2022, **3**, 5836–5844.
10 P. Biswas, H. K. Datta and P. Dastidar, *Chem. Commun.*, 2022, **58**, 969–972.
11 B. Singh, V. Sharma, R. Kumar and D. Sharma, Food Hydrocoll, *Health*, 2023, **3**, 100137.
12 N. Alam, N. Ojha, S. Kumar and D. Sarma, *ACS Sustainable Chem. Eng.*, 2023, **11**, 2658–2669.
13 S. Dhibar, A. Dey, A. Dey, S. Majumdar, A. Mandal, P. P. Ray and B. Dey, *New J. Chem.*, 2019, **43**, 15691–15699.
14 G. Lepcha, T. Singha, S. Majumdar, A. K. Pradhan, K. S. Das, P. K. Datta and B. Dey, *Dalton Trans.*, 2022, **51**, 13435–13443.
15 H. Su, S. Zhu, M. Qu, R. Liu, G. Song and H. Zhu, *J. Phys. Chem. C*, 2019, **123**, 15685–15692.
16 F. Houard, G. Cucinotta, T. Guizouarn, Y. Suffren, G. Calvez, C. Daiguebonne, O. Guillou, F. Artzner, M. Mannini and K. Bernot, *Mater. Horiz.*, 2023, **10**, 547–555.
17 K. Lalitha, Y. S. Prasad, V. Sridharan, C. U. Maheswari, G. John and S. Nagarajan, *RSC Adv.*, 2015, **5**, 77589–77594.
18 T. Zhao, S. Chen, K. Kang, J. Ren and X. Yu, *Langmuir*, 2022, **38**, 1398–1405.
19 R. Kyarikwal, N. Malviya, A. Chakraborty and S. Mukhopadhyay, *ACS Appl. Mater. Interfaces*, 2021, **13**, 59567–59579.
20 W. Fang, Y. Zhang, J. Wu, C. Liu, H. Zhu and T. Tu, *Chem. – Asian J.*, 2018, **13**, 712–729.
21 Q. Feng, K. Wan, T. Zhu, X. Fan, C. Zhang and T. Liu, *ACS Appl. Mater. Interfaces*, 2022, **14**, 4542–4551.
22 S. Dhibar, A. Dey, A. Dey, S. Majumdar, D. Ghosh, P. P. Ray and B. Dey, *ACS Appl. Electron. Mater.*, 2019, **1**, 1899–1908.
23 H. Wang, Y. Zhang, J. Xiong, D. Zhang, H. Lin and Y. Chen, *J. Mater. Sci.*, 2022, **57**, 8016–8028.
24 Y. Li, J. Wen, Z. Xue, X. Yin, L. Yuan and C. Yang, *J. Hazard. Mater.*, 2022, **426**, 127809.
25 R. El Kurdi, M. Chebl, M. Sillanpää, H. El-Rassy and D. Patra, *Mater. Today Commun.*, 2021, **28**, 102707.
26 S. Huang, X. Liu, Q. Hu, T. Wei, J. Wang, H. Chen and C. Wu, *ACS Appl. Mater. Interfaces*, 2019, **12**, 2991–2998.
27 H. L. Yang, X. W. Sun, Y. M. Zhang, Z. H. Wang, W. Zhu, Y. Q. Fan, T. B. Wei, H. Yao and Q. Lin, *Soft Matter*, 2019, **15**, 9547–9552.
28 D. Türkmen, M. Bakhshpour, S. Akgönüllü, S. Aşır and A. Denizli, *Front. Sustainable*, 2022, **3**, 765592.
29 S. Huseynli, M. Bakhshpour, T. Qureshi, M. Andac and A. Denizli, *Polymers*, 2020, **12**, 1149–1163.
30 P. C. Nagajyoti, K. D. Lee and T. V. M. Sreekanth, *Environ. Chem. Lett.*, 2010, **8**, 199–216.
31 S. Sobhanardakani, *Mar. Pollut. Bull.*, 2017, **123**, 34–38.
32 N. S. Hosseini, S. Sobhanardakani, M. Cheraghi, B. Lorestani and H. Merrikhpour, *Environ. Sci. Pollut. Res.*, 2020, **27**, 13301–13314.
33 S. Mitra, A. J. Chakraborty, A. M. Tareq, T. B. Emran, F. Nainu, A. Khusro, A. M. Idris, M. U. Khandaker, H. Osman, F. A. Alhumaydhi and J. Simal-Gandara, *J. King Saud Univ., Sci.*, 2022, **34**, 101865.
34 R. Ganesamoorthy, V. K. Vadivel, R. Kumar, O. S. Kushwaha and H. Mamane, *J. Cleaner Prod.*, 2021, **329**, 129713.
35 M. S. Salman, H. Znad, M. N. Hasan and M. M. Hasan, *Microchem. J.*, 2021, **160**, 105765.
36 M. R. Awual, *Mater. Sci. Eng., C*, 2019, **101**, 686–695.
37 M. R. Awual, *J. Environ. Chem. Eng.*, 2019, **7**, 103124.
38 M. N. Hasan, M. S. Salman, A. Islam, H. Znad and M. M. Hasan, *Microchem. J.*, 2021, **161**, 105800.
39 M. R. Awual, *J. Environ. Chem. Eng.*, 2019, **7**, 103087.
40 M. R. Awual, *J. Environ. Chem. Eng.*, 2019, **7**, 103378.
41 M. R. Awual, M. M. Hasan, A. Islam, M. M. Rahman, A. M. Asiri, M. A. Khaleque and M. C. Sheikh, *J. Cleaner Prod.*, 2019, **231**, 214–223.
42 N. Malviya, C. Sonkar, R. Ganguly, D. Bhattacherjee, K. P. Bhabak and S. Mukhopadhyay, *ACS Appl. Mater. Interfaces*, 2019, **11**, 47606–47618.
43 N. Malviya, R. Ranjan, C. Sonkar, S. M. Mobin and S. Mukhopadhyay, *ACS Appl. Nano Mater.*, 2019, **2**, 8005–8015.
44 N. Malviya, C. Sonkar, B. K. Kundu and S. Mukhopadhyay, *Langmuir*, 2018, **34**, 11575–11585.
45 N. Malviya, C. Sonkar, R. Ganguly and S. Mukhopadhyay, *Inorg. Chem.*, 2019, **58**, 7324–7334.
46 R. Kyarikwal, B. K. Kundu, A. Chakraborty and S. Mukhopadhyay, *Mater. Chem. Front.*, 2022, **6**, 2835–2847.
47 A. Chakraborty, S. Sarkar, R. Kyarikwal, P. Nag, S. R. Vennapusa and S. Mukhopadhyay, *ACS Appl. Polym. Mater.*, 2022, **4**, 8118–8126.

48 C. Santhosh, R. Nivetha, P. Kollu, V. Srivastava, M. Sillanpää, A. N. Grace and A. Bhatnagar, *Sci. Rep.*, 2017, **7**, 14107.
49 M. R. Awual, M. N. Hasan, M. M. Hasan, M. S. Salman, M. C. Sheikh, K. T. Kubra, M. S. Islam, H. M. Marwani, A. Islam, M. A. Khaleque and R. M. Waliullah, *Sep. Purif. Technol.*, 2023, **319**, 124088.
50 K. T. Kubra, M. M. Hasan, M. N. Hasan, M. S. Salman, M. A. Khaleque, M. C. Sheikh, A. I. Rehan, A. I. Rasee, R. M. Waliullah, M. E. Awual and M. S. Hossain, *Colloids Surf., A*, 2023, **667**, 131415.
51 M. S. Salman, M. N. Hasan, M. M. Hasan, K. T. Kubra, M. C. Sheikh, A. I. Rehan, R. M. Waliullah, A. I. Rasee, M. E. Awual, M. S. Hossain and A. K. Alsukaibi, *J. Mol. Struct.*, 2023, **1282**, 135259.
52 M. N. Hasan, M. S. Salman, M. M. Hasan, K. T. Kubra, M. C. Sheikh, A. I. Rehan, A. I. Rasee, M. E. Awual, R. M. Waliullah, M. S. Hossain and A. Islam, *J. Mol. Struct.*, 2023, **1276**, 134795.
53 M. Mohammed, R. D. Chakravarthy and H. C. Lin, *Mol. Syst. Des. Eng.*, 2022, **7**, 1336–1343.
54 A. Zhang, Y. Zhang, Z. Xu, Y. Li, X. Yu and L. Geng, *RSC Adv.*, 2017, **7**, 25673–25677.
55 M. A. Haidekker, T. P. Brady, D. Lichlyter and E. A. Theodorakis, *Bioorg. Chem.*, 2005, **33**, 415–425.
56 H. R. Bhat and P. C. Jha, *ChemistrySelect*, 2017, **2**, 2732–2739.
57 M. Sowmiya, A. K. Tiwari and S. K. Saha, *J. Photochem. Photobiol., A*, 2011, **218**, 76–86.
58 J. Liu, Y. Q. Fan, S. S. Song, G. F. Gong, J. Wang, X. W. Guan, H. Yao, Y. M. Zhang, T. B. Wei and Q. Lin, *ACS Sustainable Chem. Eng.*, 2019, **7**, 11999–12007.
59 Y. L. Xu, C. T. Li, Q. Y. Cao, B. Y. Wang and Y. A. Xie, *Dyes Pigm.*, 2017, **139**, 681–687.
60 Y. Zhang, C. Liang, H. Shang, Y. Ma and S. Jiang, *J. Mater. Chem. C*, 2013, **1**, 4472–4480.
61 E. Beltrán, M. Garzoni, B. Feringan, A. Vancheri, J. Barbera, J. L. Serrano, G. M. Pavan, R. Gimenez and T. Sierra, *Chem. Commun.*, 2015, **51**, 1811–1814.
62 C. T. Lee, W. T. Yang and R. G. Parr, *Phys. Rev. B: Condens. Matter Mater. Phys.*, 1988, **37**, 785–789.
63 S. Grimme, J. Antony, S. Ehrlich and H. Krieg, *J. Chem. Phys.*, 2010, **132**, 154104.
64 L. Tian and C. Feiwu, *J. Comput. Chem.*, 2012, **33**, 580–592.
65 E. Saeedreza, L. Tian, K. Holger and E. Hamidreza, *J. Comput. Chem.*, 2019, **40**, 2868–2881.
66 Y. Ding, F. Zhang, J. Xu, Y. Miao, Y. Yang, X. Liu and B. Xu, *RSC Adv.*, 2017, **7**, 28754–28762.
67 A. Chowdhury, S. K. Das, S. Mondal, S. Ruidas, D. Chakraborty, S. Chatterjee, M. K. Bhunia, D. Chandra, M. Hara and A. Bhaumik, *Environ. Sci.: Nano*, 2021, **8**, 2641–2649.
68 Y. Ding, F. Zhang, J. Xu, Y. Miao, Y. Yang, X. Liu and B. Xu, *RSC Adv.*, 2017, **7**, 28754–28762.
69 A. Artemenko, A. Shchukarev, P. Štenclová, T. Wågberg, J. Segervald, X. Jia and A. Kromka, *IOP Conf. Ser.: Mater. Sci. Eng.*, 2021, **1050**, 012001.
70 A. D. Martínez-Iniesta, A. Morelos-Gómez, E. Muñoz-Sandoval and F. López-Urías, *RSC Adv.*, 2021, **11**, 2793–2803.
71 R. Liu, L. Zuo, X. Huang, S. Liu, G. Yang, S. Li and C. Lv, *Microchim. Acta*, 2019, **186**, 1–8.